CRYSTAL GROWTH & DESIGN

Article

pubs.acs.org/crystal

Crystal Growth and Raman Spectroscopy Study of $Sm_{1-x}La_xFe_3(BO_3)_4$ Ferroborates

Evgeniya Moshkina,*[,†,‡] Alexander Krylov,[†] Svetlana Sofronova,[†] Irina Gudim,[†] and Vladislav Temerov[†]

[†]Kirensky Institute of Physics, Federal Research Center KSC SB RAS, Krasnoyarsk, 660036, Russia

[‡]Siberian State Aerospace University, Krasnoyarsk, 660037, Russia

Supporting Information

ABSTRACT: $Sm_{1-x}La_xFe_3(BO_3)_4$ (x = 0, 0.75) single crystals were synthesized using the flux method. The crystal nucleation procedure and flux parameters are reported. Conditions for growing the $Sm_{1-x}La_xFe_3(BO_3)_4$ (x = 0, 0.75) single crystals are described. The prepared crystals were studied by Raman spectroscopy in the temperature range of T = 10−300 K. The spectral region corresponding to temperatures of T = 10−55 K, which involves the temperatures of the magnetic phase transition T_N = 32 K for x = 0 and T_N = 31 K for x = 0.75, was thoroughly analyzed. Anomalies related to the magnetic ordering established in both compounds were found. The main changes occur in the low-wavenumber region (up to 100 cm^{-1}), where the mode corresponding to magnon scattering arises. This mode is shown to have the internal structure indicative of the occurrence of unstable vibrations (40−80 cm^{-1}). The results obtained are analyzed by calculating the empirical lattice dynamics in $Sm_{1-x}La_xFe_3(BO_3)_4$ with x = 0 and x = 1.

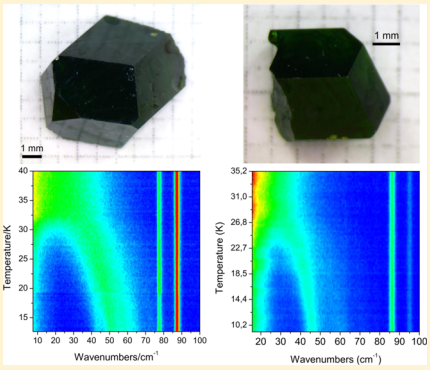

INTRODUCTION

Rare-earth huntites are the broad class of compounds with different degrees of substitution of metal and rare-earth ions. The properties of these compounds have been intensively studied for the last two decades. The interest in huntites is due to the wide range of characteristics, including the magnetoelectric effect, magnetic ordering, spin reorientation, and high optical activity. Huntites are currently used as laser active media. The discovery of the magnetoelectric effect in huntites has determined a new direction for application of these materials. Despite a significant number of studies on these compounds, some of their properties, in particular, the nature of magnetoelectric polarization, remain unclear. An effective technique for studying these properties is synthesis and investigations of solid solutions with different degrees of substitution of metal and rare-earth ions. Here, we investigate the $Sm_{1-x}La_xFe_3(BO_3)_4$ (x = 0, 0.75) solid solution with nonmagnetic ions substituted for magnetic ones.

The high-temperature phase of crystals with the huntite structure is characterized by the trigonal symmetry (sp. gr. $R32$). Depending on the ratio between rare-earth and metal ion radii, the structural phase transition to the phase with the $P3_121$ space symmetry can occur in huntites.[1] This transition is not observed in $Sm_{1-x}La_xFe_3(BO_3)_4$ (x = 0, 0.75); at low temperatures, these crystals are characterized by the trigonal symmetry (sp. gr. $R32$).[2]

The huntite structure contains quasi-low-dimensional elements, specifically, chains consisting of metal−oxygen polyhedrons (Figure 1). The interchain coupling plays a decisive role; the elements are characterized by the stronger exchange coupling. The exchange coupling between chains is weak. Thus,

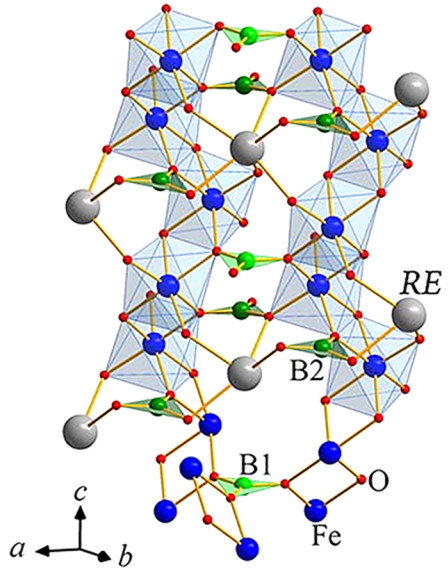

Figure 1. Huntite structure.

during the magnetic phase transition, many huntite compounds exhibit magnetic ordering only within metal ion chains (Fe); rare-earth ions are disordered and only magnetized by the Fe subsystem. The magnetic moments of Fe ions in $Sm_{1-x}La_xFe_3(BO_3)_4$ (x = 0, 0.75) are ordered antiferromagneti-

Received: July 20, 2016
Revised: October 23, 2016
Published: October 24, 2016

DOI: 10.1021/acs.cgd.6b01079
Cryst. Growth Des. 2016, 16, 6915−6921

Table 1. Parameters of the Fluxes

flux composition in the quasi-binary form(100-n) mass % [$Bi_2Mo_3O_{12}$ + pB_2O_3 + qSm_2O_3 + rLa_2O_3] + n mass % $Sm_{1-x}La_xFe_3(BO_3)_4$								
crystal	p	q	r	n	T_{sat}, °C	dT_{sat}/dn, °C/mass %	ΔT_{met}, °C	Accompanying phases
$SmFe_3(BO_3)_4$	3	0.6	0	25	962	2.5	12	α-Fe_2O_3·Fe_3BO_6
$Sm_{0.25}La_{0.75}Fe_3(BO_3)_4$	3	0.15	0.45	25	965	4.0		

cally at T_N = 32 K (x = 0) and T_N = 31 K (x = 0.75) and lie in the basal plane *ab*. The magnetic moments of samarium ions biased by the exchange field of the Fe subsystem also lie in the basal plane. Upon substitution of nonmagnetic La ions for Sm ions, the antiferromagnetic interaction between the iron and rare-earth subsystems weakens, which is confirmed by an increase in the total magnetic moment.[2]

Here, we report on the synthesis of $Sm_{1-x}La_xFe_3(BO_3)_4$ (x = 0, 0.75) single crystals and Raman spectroscopy study of the magnetic phase transitions in them. Huntite compounds are characterized by the internal magnetic field (exchange field) induced by the magnetic order established in the samples below the temperature of the magnetic phase transition. This fact allows us to observe the Raman spectra variations caused by the established magnetic order without external magnetic field.[3] This technique makes it possible to record even minor crystal structure variations and to reveal the character of ion bonds, which can arise upon magnetic ordering and magnetoelectric polarization.[2,4]

The features of the huntite vibrational spectrum caused by the magnetic phase transitions have been understudied. Adem et al.[5] studied Raman spectra of the $TbFe_3(BO_3)_4$ crystal. It was observed that the magnetic phase transition is accompanied by the shift of the 200 and 260 cm^{-1} lines, while the rest lines do not significantly move. The authors attributed this effect to the permittivity anomaly at the magnetic phase transition and the permittivity dependence of splitting of the longitudinal and transversal vibration modes.

Also, attractive features were observed at the magnetic phase transition in $Nd_{1-x}Ho_xFe_3(BO_3)_4$ solid solutions, specifically, the occurrence of new modes in the ranges of 600−650 cm^{-1} (x = 0.25, 0.5) and 700−750 cm^{-1} (x = 0.75).[6] Meanwhile, pure $HoFe_3(BO_3)_4$ and $NdFe_3(BO_3)_4$ compounds did not exhibit any features below the temperature of the magnetic phase transition in the spectral range of 600−800 cm^{-1}.[6] Such anomalies are apparently typical only of solid solutions and explained by local distortions caused by the significant difference between holmium and neodymium ionic radii.

The technique used to examine the observed peculiarities plays an important role. In particular, in $Nd_{1-x}Ho_xFe_3(BO_3)_4$ solid solutions, no anomalies of infrared (IR) spectra in the spectral range of 600−800 cm^{-1} were found.[7,8] Meanwhile, high-resolution Raman spectroscopy allows one to observe even minor crystal structure changes upon magnetic ordering.

CRYSTAL GROWTH

Since rare earth borates $ReMe_3(BO_3)_4$ with Re = (Y, Pr−Lu) and Me = (A1, Ga, Cr, Fe, Sc) melt incongruently, their crystals are grown using flux techniques.

The solvent systems used previously for this purpose were PbF_2−B_2O_3, Bi_2O_3−B_2O_3, $Li_2B_4O_7$, BaO−B_2O_3, and K_2SO_4−$3MoO_3$. However, they cannot ensure the crystal size required for complex measurements.

At present, rare-earth borate single crystals are usually grown from the fluxes based on potassium trimolibdate $K_2Mo_3O_{10}$. However, Boldyrev et al.[9] found significant K and Mo inclusions in the grown crystals.

In 2004, the research team from the Kirensky Institute of Physics, Russian Academy of Sciences, Siberian Branch, proposed to grow $ReAl_3(BO_3)_4$ and $ReFe_3(BO_3)_4$ single crystals from new fluxes based on bismuth trimolibdate $Bi_2Mo_3O_{12}$ with the ratio between the of Bi_2O_3 and MoO_3 oxides corresponding to stoichiometric bismuth trimolibdate $Bi_2Mo_3O_{12}$ with the low melting point and low viscosity.[10,11] In these fluxes, Bi_2O_3 and MoO_3 are bound more strongly than K_2O and MoO_3. Therefore, the degree of substitution of bismuth and molybdenum for the rare-earth element in the grown crystal is low.[9]

$Sm_{1-x}La_xFe_3(BO_3)_4$ (x = 0, 0.75) single crystals were synthesized using the flux method. Below, we describe the crystal nucleation procedure and report the flux parameters.

Phase Formation. For the sake of convenience, the formula of the flux system under study can be written in the quasi-binary form

$$(100 - n)\%\text{mass}\ (Bi_2Mo_3O_{12} + pB_2O_3 + qSm_2O_3 + rLa_2O_3) + n\%\text{mass}\ Sm_{1-x}La_xFe_3(BO_3)_4$$

where n is the crystal-forming oxide concentration corresponding to $Sm_{1-x}La_xFe_3(BO_3)_4$ stoichiometry and p, q, and r are the parameters of the ratio between the crystal-forming oxides in the solution.

The fluxes in a mass of 150 g with different p, q, r, and n values were prepared at T = 1000−1100 °C by sequential melting of the oxides [Bi_2O_3 (reagent grade), MoO_3 (analytical grade)], B_2O_3 (special-purity grade), and [Fe_2O_3 (special-purity grade), Sm_2O_3 (SmO-E), La_2O_3 (LaO-L)] (domestic reagents) in a cylindrical platinum crucible 50 mm in diameter and 60 mm in height. The crucible with the prepared flux was loaded into a furnace with a vertical temperature gradient of 2−3 °C/cm. The crucible bottom was hot. Homogenization of the solution occurred within 24 h at 1000 °C; then, a platinum rod 4 mm in diameter was immersed in the solution. In 1−2 h, the rod was withdrawn, and the nucleation on it was estimated. The probing was performed at temperatures down to $T \approx$ 850 °C with a 10−20 °C temperature step without solution superheating.

It was established that the only phase crystallizing at $p = q = r$ = 0 and n = 10−25% in the temperature range of 1000−850 °C is hematite (α-Fe_2O_3). With an increase in the B_2O_3 and $(Sm, La)_2O_3$ concentrations to p = 2 and $(q + r)$ = 0.4, hematite remains in the high-temperature phase; however, at low temperatures, Fe_3BO_6 crystallites arise. Trigonal $(Sm, La)Fe_3(BO_3)_4$ becomes a high-temperature phase only at p = 2.5—3 and $(q + r)$ = 0.5−0.6. The α-Fe_2O_3 and Fe_3BO_6 phases keep forming but in the lower part of the temperature range. The main parameters of crystallization of the fluxes with p = 3 and $(q + r)$ = 0.6 are given in Table 1. At the specified concentrations of the crystal-forming oxides, the flux saturation temperature was below 1000 °C, which excludes uncontrolled variations in the crystallization conditions during the work with an open crucible. The metastable zone width ΔT_{met} = 12 °C

DOI: 10.1021/acs.cgd.6b01079
Cryst. Growth Des. 2016, 16, 6915−6921

corresponds to the 20-h exposure of the flux in the supercooled state. As the exposure time is increased, ΔT_{met} remains nearly constant. Below 870 °C, crystallization is ineffective because of the increasing flux viscosity and decreasing allowed supercooling (i.e., ΔT_{met} narrowing).

Table 2. Parameters of the Born−Karman Model for Different Pairs of Ions

ion−ion	A (10^{-18} J/Å^2)	B (10^{-18} J/Å^2)
La(Sm)−B	300.17	0.39
La(Sm)−Fe	250.17	0.38
La(Sm)−O	310.17	0.34
B−Fe	350.17	0.35
B−O	350.17	0.268
Fe−Fe	250.17	0.383
Fe−O	336.17	0.365
O−O	306.17	0.389
B−B	250.17	0.34

Spontaneous Nucleation. First, the saturation temperature was determined accurately to ±2 °C using probe crystals. Then, a clean platinum rod was immersed in the flux to a depth of 15−20 mm at a temperature of T = 1000 °C and rotated for a period of 1 min at a rate of 30 rpm. The furnace temperature was reduced to $T = T_{sat} - 15$ °C. In 2 h, the rod was withdrawn from the furnace. Crystal nucleation was observed in the rapidly cooled thin solution layer on the rod. Then, the rod was immersed in the flux again at the same temperature ($T = T_{sat} - 15$ °C) and rotated in the same regime. During the next 24 h, 10−30 high-quality crystals 0.5−2 mm in size were grown. These crystals were used as a seed material.

Seeded Growth of Crystals. The rod with four high-quality seeds ∼1 mm in size was placed above the flux at T = 1050 °C. Then, the temperature was reduced to $T = T_{sat} + 7$ °C, and the rod was immersed in the solution to a depth of 15−20 mm and rotated with a period of 1 min at a rate of 30 rpm. In 15 min, the temperature was reduced to $T = T_{sat} - 5$ °C. After that, the temperature was gradually reduced by 1−2 °C daily. The growth was finished in a period between 9−13 days. The rod was elevated above the solution and cooled to room temperature in the switched-off furnace. The obtained crystals were 6−10 mm in size, which is sufficient for further investigations (Figure 2).

RAMAN SPECTROSCOPY STUDY

Experimental Section. Raman spectra of the $Sm_{1-x}La_xFe_3(BO_3)_4$ (x = 0, 0.75) single crystals were recorded on a Horiba Jobin Yvon T64000 triple spectrometer equipped with a liquid nitrogen cooled charge-coupled device detector operating in the subtractive dispersion mode in the back-scattering geometry. As an excitation light source, a Spectra-Physics Stabilite 2017 Ar+ ion laser with λ = 514.5 nm and a power of 7 mW on a sample was used.

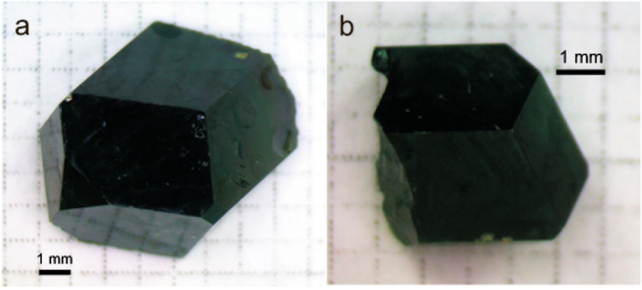

Figure 2. Synthesized (a) $SmFe_3(BO_3)_4$ and (b) $Sm_{0.25}La_{0.75}Fe_3(BO_3)_4$ crystals.

Temperature measurements were performed on an ARS CS204-X1.SS closed-cycle helium cryostat in the temperature range of 10−300 K. The temperature was monitored using a LakeShore DT-6SD1.4L silicon diode. During the experiments, the cryostat was evacuated to 10^{-6} mbar. To investigate low-wavenumber spectra, spectroscopic measurements in the subtractive dispersion mode were performed; the attained low-wavenumber limit was 8 cm^{-1}. Deformation of the low-wavenumber spectral edge by an optical slit, which sometimes smears true features of the spectra, was carefully eliminated by rigorous optical alignment. The CCD pixel coverage in the additive dispersion mode was as fine as 0.3 cm^{-1}, but it was limited by the spectral resolution of the spectrometer (2 cm^{-1}).

Temperature experiments were carried out in the dynamic regime upon sample temperature variation at a rate of 0.7 K/min. The measured temperature uncertainty at the given rate estimated as a difference between adjacent measurements was ±0.12 K in one spectrum measurement. The total time for accumulating one spectrum was about 30 s. The spectra were acquired with a temperature step of 0.5 K. The measurement protocol was similar to that described in refs 12 and 13.

The spectra were deconvolved into separate spectral lines to obtain quantitative information. The line shapes were described using the Lorentz function.[14]

To interpret the experimental results, we calculated the empirical lattice dynamics of pure $SmFe_3(BO_3)_4$ and $LaFe_3(BO_3)_4$ ferroborates using the LADY software package (Table 1).[15]

Results and Discussion. Raman spectra of the $Sm_{1-x}La_xFe_3(BO_3)_4$ (x = 0, 0.75) single crystals were obtained in the temperature range of T = 10−300 K. As expected structural phase transition $R32 \rightarrow P3_121$ was not detected in these crystals. In the temperature range of 35−300 K, the Raman spectra have no peculiarities, and the temperature behavior of spectral lines agrees well with the theoretical temperature dependences. The latter were calculated with regard to the three-phonon interactions caused by lattice anharmonism in the absence of phase transitions.[16] Below the temperatures of T_N = 32 K (x = 0) and T_N = 31 K (x = 0.75), deviations from the theoretical dependences were found, which are related to the magnetic phase transition. Given this, we focused on the experimental study of the Raman spectra of the $Sm_{1-x}La_xFe_3(BO_3)_4$ (x = 0, 0.75) crystals below T = 55 K.

The experimental Raman spectra of several huntite compounds with different rare-earth ions of $ReFe_3(BO_3)_4$ family were found to have the same structure: the vibrational spectra are formed by internal vibrations of the BO_3, FeO_6, and ReO_6 groups. Since these groups are mainly localized, the radius of a rare-earth ion only slightly affects the vibrational spectrum, except for the low wavenumber regions, where the modes are mainly related to the rare-earth ion.[1] Therefore, the spectra of huntites with different compositions are similar, and one should not expect a significant difference between the spectra of the solid solutions. As expected, the calculated vibrational spectra of the $SmFe_3(BO_3)_4$ and $LaFe_3(BO_3)_4$ crystals significantly differ. The calculations were performed

DOI: 10.1021/acs.cgd.6b01079
Cryst. Growth Des. 2016, 16, 6915−6921

for both crystals with the trigonal structure, space group *R*32; the atomic coordinates were borrowed from ref 17.

The greatest change in the Raman spectra of the huntites under study is observed in the low-wavenumber spectral range (Figure 3) due to the occurrence of the low-wavenumber

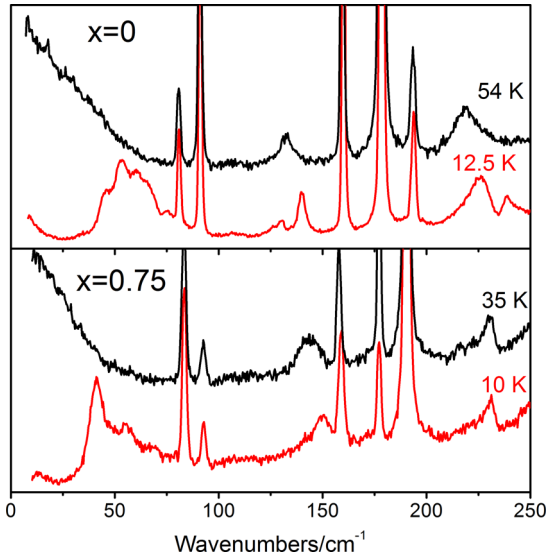

Figure 3. Experimental Raman spectra of the $Sm_{1-x}La_xFe_3(BO_3)_4$ (x = 0, 0.75) single crystals.

mode, which is caused by magnetoelastic scattering and strongly temperature-dependent below the Neel temperature. The detailed analysis of this magnon revealed the internal structure consisting of unstable vibrations (40−80 cm^{-1} at x = 0 and 30−75 cm^{-1} at x = 0.75 (Figures 4 and 5)). This is consistent with the Raman spectroscopy data on other compounds in the rare-earth ferroborate family (Re = Nd, Gd, Y, Tb).[1] Indeed, when the long-range magnetic order is established in the iron subsystem, the Raman spectra demonstrate the growth of a broad-structured scattering band associated with two-magnon Raman scattering, which is followed by the formation of a magnon pair with wave vectors $\vec{k}$ and $-\vec{k}$.[1] The center position of this broad magnetic scattering band in the spectrum of the investigated $Sm_{1-x}La_xFe_3(BO_3)_4$ (x = 0, 0.75) huntites depends on the radius of a rare-earth ion. This confirms the above-made assumption about the directly proportional dependence of the center position on ionic radii (R(Nd) = 0.983 Å, R(Sm) = 0.958 Å, and R(La) = 1.032 Å).[1] Another typical feature of the low-wavenumber Raman spectra of the magnetically ordered ferroborates is the low-frequency peak (10−18) cm^{-1} corresponding to spin-flip scattering on single rare-earth ion moments.[1] In this study, the low-frequency peak was not observed. This result is also consistent with the magnetization measurement data on $Sm_{1-x}La_xFe_3(BO_3)_4$ (x = 0, 0.75), where the spin-flip transitions do not occur.[2]

Along with the occurrence of the low-wavenumber broad band, there are some other anomalies in the spectral range of 100−500 cm^{-1} at the temperature of the magnetic phase transition.

The temperature dependence of the 131 cm^{-1} line contains a noticeable inflection at the temperature of the magnetic phase transition (Figure 7). In the paramagnetic phase, this dependence was approximated by the theoretical dependence

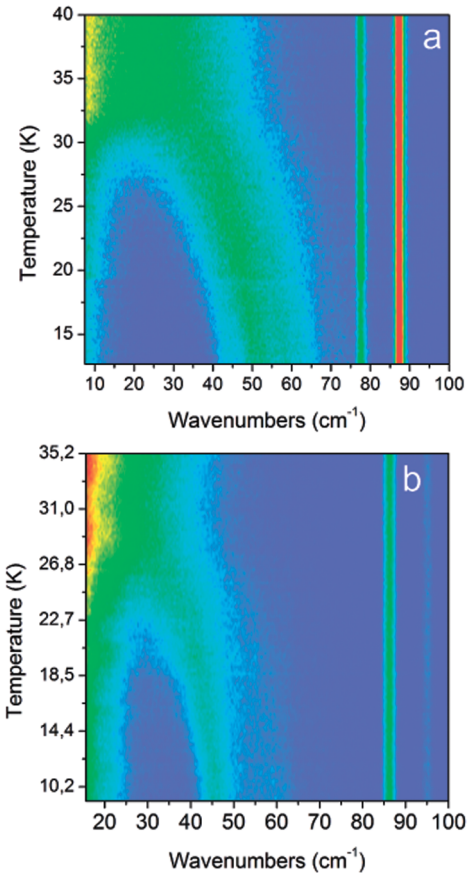

Figure 4. Low-wavenumber range of the Raman spectra for $Sm_{1-x}La_xFe_3(BO_3)_4$ with (a) x = 0 and (b) 0.75.

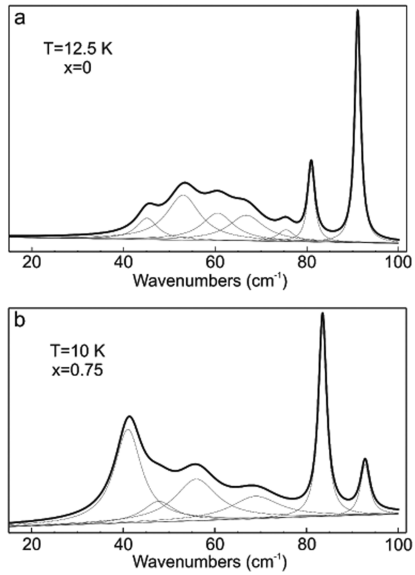

Figure 5. Internal structure of the low-wavenumber modes of $Sm_{1-x}La_xFe_3(BO_3)_4$ with (a) x = 0 and (b) 0.75.

calculated with regard to the three-phonon interactions, which result from anharmonism of the lattice vibrations.[16] It can be seen from the difference between the experimental and theoretical curves below the transition temperature (inset in Figure 7) that the deviation from the theoretical curve starts growing at a temperature of T_N = 32 K and attains the value of

DOI: 10.1021/acs.cgd.6b01079
Cryst. Growth Des. 2016, 16, 6915−6921

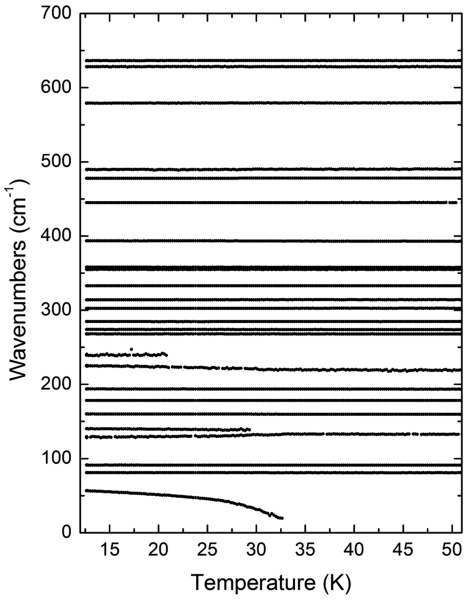

Figure 6. Temperature dependences of the positions of Raman lines for $SmFe_3(BO_3)_4$.

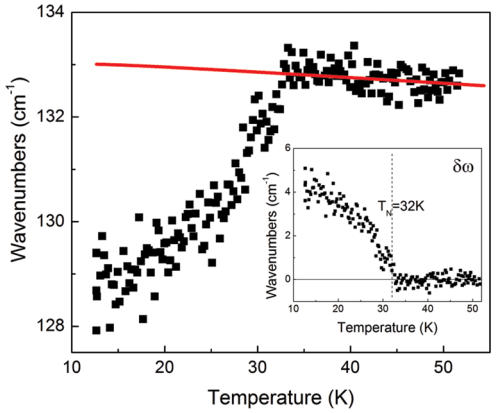

Figure 7. Temperature dependence of the position of the 131 cm^{-1} Raman line for $SmFe_3(BO_3)_4$. The solid line shows approximation to the experimental data with regard to the three-phonon interactions caused by lattice anharmonism in the absence of phase transitions with the use of the data in the paramagnetic phase. Inset: difference between the approximation and experiment.

$\Delta\nu$ = 4 cm^{-1} at T = 12.5 K. The same behavior was observed in $TbFe_3(BO_3)_4$, where the shifts of the 200 and 260 cm^{-1} lines were detected at the magnetic phase transition associated with the permittivity anomaly and permittivity dependence of splitting of the longitudinal and transverse vibration modes.[5]

The occurrence of new lines, 134 and 245 cm^{-1}, is observed below the phase transition temperature T_N = 32 K (Figure 6). There is a kink in the temperature dependence of the 220 cm^{-1} line closest to the 245 cm^{-1} line at the phase transition temperature (Figure S2). The deviation from the theoretical curve attains the same value ($\Delta\nu$ = 4 cm^{-1}) as for the 131 cm^{-1} mode, but the position of the 220 cm^{-1} line center shifts to the large wavenumber region with decreasing temperature.

The sensitivity to the magnetic phase transition observed as inflections in the temperature dependences of the line center positions (angle changes) is demonstrated by the 333, 445, and 477 cm^{-1} lines (Figure S3), but here the deviations of wavenumbers from the theoretical curves are much smaller than for the lines discussed above. The deviations are $\Delta\nu$(333 cm^{-1}) = 0.25 cm^{-1}, $\Delta\nu$(445 cm^{-1}) = 0.15 cm^{-1}, and $\Delta\nu$(477 cm^{-1}) = 0.3 cm^{-1}. It should be noted that all these lines are characterized by wavenumber lowering below the phase transition temperature. This behavior can be indicative of the change in the character of ionic bonds corresponding to the wavenumbers or of the decrease in the interionic distances upon the magnetic ordering of the crystal.

The variations in the Raman spectra related to the magnetic phase transition were also observed by the behavior of the 178 and 302 cm^{-1} lines. Although there are no anomalies in the temperature dependence of the line positions and widths at the Neel temperature, the relative intensities of these lines have inflections at T_N = 32 K (Figure S4).

Slight inflections in the temperature dependences of the positions of some lines are observed upon vibrations of the BO_3 group (viz. 900−1000 cm^{-1}, 1150−1400 cm^{-1}). These inflections correspond to tuning to the changed BO_3 group lattice upon magnetic ordering.

Despite the similarity of the magnetic properties of the ordered $SmFe_3(BO_3)_4$ and $Sm_{0.25}La_{0.75}Fe_3(BO_3)_4$ phases,[2] their Raman spectra contain various anomalies at the magnetic phase transitions. Figures 8 and S5 illustrate temperature transformations of the Raman spectra of $Sm_{0.25}La_{0.75}Fe_3(BO_3)_4$. The main changes are observed in the spectral range of 158−161 cm^{-1} (Figure 9). The changes in the Raman spectra of $SmFe_3(BO_3)_4$ consist of the shift of the line positions and kinks in the temperature dependences of the relative intensity of some spectral lines in the range of 100−500 cm^{-1}. In contrast to the first compound, in $Sm_{0.25}La_{0.75}Fe_3(BO_3)_4$, the magnetic ordering affects not only the line positions but also the line width of the 160 cm^{-1} mode (Figure 9b). Below the magnetic phase transition temperature, this line significantly broadens. At a temperature of T = 12 K, the line width increases by 60% relative to the value above the Neel temperature T_N = 31 K.

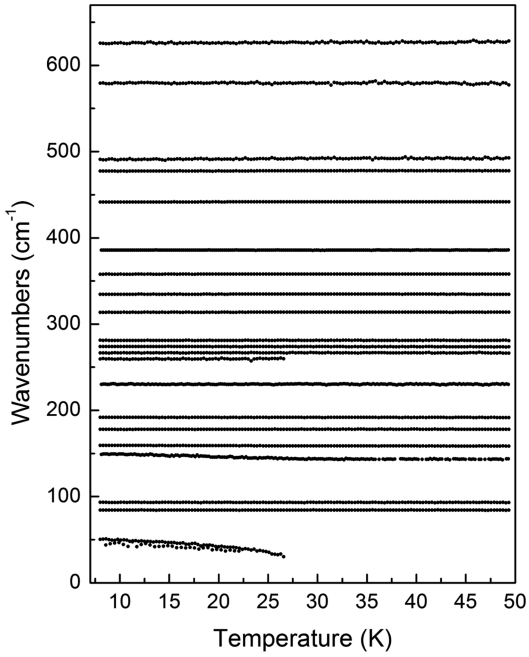

Figure 8. Temperature dependences of the positions of the (20−700) cm^{-1} Raman line for $Sm_{0.25}La_{0.75}Fe_3(BO_3)_4$.

DOI: 10.1021/acs.cgd.6b01079
Cryst. Growth Des. 2016, 16, 6915−6921

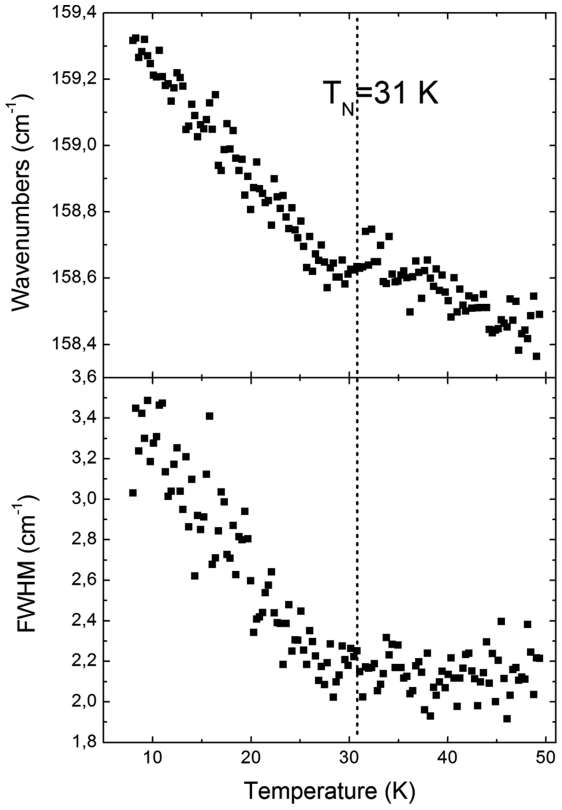

Figure 9. Temperature dependences of the position and line width of the 160 cm^{-1} Raman line for $Sm_{0.25}La_{0.75}Fe_3(BO_3)_4$.

In accordance with the group theory analysis, the huntite spectra contain vibrations with the A_1 and A_2 symmetries and doubly degenerated vibrations E. The difference between the longitudinal and transverse vibrations with the E symmetry in the spectral range 80−900 cm^{-1} of these compounds is smaller than 15 cm^{-1}.[1] The difference between some E_{LO} and E_{TO} modes, including 160, 270, 391, and 443 cm^{-1}, in $GdFe_3(BO_3)_4$, is smaller than 1 cm^{-1}. As was mentioned above, the huntite spectra undergo minor variations upon substitution of the rare-earth ion, and the spectra of all the investigated compounds contain the (158−160) cm^{-1} line. It is very likely that in $Sm_{0.25}La_{0.75}Fe_3(BO_3)_4$, similar to $GdFe_3(BO_3)_4$, the difference between the E_{LO} and E_{TO} vibrational frequencies is insignificant. Below the temperature of the magnetic phase transition, one of the vibrations shifts (as in $TbFe_3(BO_3)_4$[5]), and, as a result, the line broadens. The observed broadening can be explained as follows. As a rule, the number of lines in the spectra of solid solutions is larger than the number allowed by the symmetry analysis for the group symmetry. Because of the irregular distribution of Sm and La ions and changes in the bond length depending on the local environment (La or Sm), the vibrational frequencies of the same structural elements become different. Probably, the magnetic phase transition affects the vibrations with preferred localization of a Sm ion stronger than those with preferred localization of a La ion. This could lead to a broadening of the 160 cm^{-1} line.

A similar broadening is observed for the 476 cm^{-1} mode line width, but, in this case, the broadening value is only 25% of the paramagnetic phase line width (Figure S6). In contrast to the 160 cm^{-1} mode, no anomalies were detected in the temperature dependence of the 476 cm^{-1} line position.

Along with the anomalies in the 100−500 cm^{-1} range corresponding to lattice vibrations and vibrations of the $[FeO_3]^{3-}$ and $[ReO_3]^{3-}$ groups in the $Sm_{0.25}La_{0.75}Fe_3(BO_3)_4$ ferroborate, the changes in the Raman spectra of this crystal were observed in the region of larger wavenumbers corresponding to internal vibrations of the $[BO_3]^{3-}$ group. There is the anomaly in the temperature dependence of the 946 cm^{-1} line position: the inflection and low-frequency shift at the Neel temperature T_N = 31 K are observed (Figure S7). The deviation of the experimental data from the calculated ones is 0.5 cm^{-1} (inset in Figure S7). Magnetic phase transition-related anomalies of the line width of this mode were not detected. The feature of the temperature dependence of the Raman spectra of the $Sm_{0.25}La_{0.75}Fe_3(BO_3)_4$ ferroborate is the sensitivity of the 1191 cm^{-1} line to the magnetic phase transition (Figure S8). The wavenumber of this mode becomes softer at the Neel temperature; at T = 10 K, the wavenumber deviation is 1 cm^{-1}.

The interesting feature of the $Sm_{0.25}La_{0.75}Fe_3(BO_3)_4$ solid solution is that the modes related to internal vibrations of the BO_3 group with wavenumbers of 946 and 1191 cm^{-1} are highly sensitive to the magnetic phase transition. Such anomalies have not been observed at the phase transitions in similar compounds. The external vibrations 131, 178, 220, 302, 333, and 445 cm^{-1} are the most sensitive to the magnetic phase transition due to the shifts of rare-earth and iron ions in the eigenvectors of these modes (Table S1).

The observed effect of shifting the line positions at the magnetic phase transition, which is similar to that demonstrated by $TbFe_3(BO_3)_4$, is attributed to the permittivity anomalies at the magnetic phase transition, which are caused by the permittivity dependence of splitting of the longitudinal and transverse vibrations. However, it remains unclear why this effect selectively affects the vibrations.

CONCLUSIONS

The $Sm_{1-x}La_xFe_3(BO_3)_4$ (x = 0, 0.75) single crystals were synthesized by the flux method. Raman spectra of the $Sm_{1-x}La_xFe_3(BO_3)_4$ (x = 0, 0.75) ferroborates in the range of T = (10−300) K were obtained. Over the entire temperature range, no changes in the spectra related to the structural phase transition were detected. The low-temperature spectral range T = (10−55) K, including the temperature of the magnetic phase transition, was thoroughly analyzed. Spectral anomalies caused by the second-order phase transition were found at temperatures of T_N = 32 K (x = 0) and T_N = 31 K (x = 0.75). These temperatures correspond to the temperatures of the magnetic phase transitions and agree well with the available data on magnetization.[2] The experimental Raman spectra were analyzed. The experimental wavenumbers and line widths of some spectral lines were theoretically approximated. Some anomalies of the spectral lines related to magnetic ordering were established. It was found that the main changes in the spectra are observed in the low-wavenumber region (up to 100 cm^{-1}): the mode related to two-magnon scattering arises. Further investigations showed that this mode has the internal structure; i.e., a set of unstable vibrations (40−80 cm^{-1}) occur. Shifts of the positions of different lines were observed for both $Sm_{1-x}La_xFe_3(BO_3)_4$ (x = 0, 0.75) compositions. Despite the similarity of the structures and compositions, the other changes related to the phase transition are different. It means that substitution of a nonmagnetic La ion affects the mechanism of magnetic ordering within Fe ionic chains. The weakening of the

DOI: 10.1021/acs.cgd.6b01079
Cryst. Growth Des. 2016, 16, 6915−6921

antiferromagnetic interaction between the Fe and rare-earth subsystems upon doping with La yields the Raman spectra anomalies caused by the changes in atomic bonds.

■ ASSOCIATED CONTENT

Supporting Information

The Supporting Information is available free of charge on the ACS Publications website at DOI: 10.1021/acs.cgd.6b01079.

Figure S1 Temperature dependencies of the Raman lines positions of $SmFe_3(BO_3)_4$ (930−1300 cm^{-1}). Figure S2 Temperature dependence of the Raman line position 222 cm^{-1} of $SmFe_3(BO_3)_4$. Figure S3 Temperature dependencies of the Raman lines positions of $SmFe_3(BO_3)_4$. Figure S4 Temperature dependencies of the Raman lines relative intensities of $SmFe_3(BO_3)_4$. Figure S5 Temperature dependencies of the Raman lines positions of $Sm_{0.25}La_{0.75}Fe_3(BO_3)_4$ (900−1500 cm^{-1}). Figure S6 Temperature dependence of 476 cm^{-1} line width of $Sm_{0.25}La_{0.75}Fe_3(BO_3)_4$. Figure S7 Temperature dependencies of 946 cm^{-1} Raman line position of $Sm_{0.25}La_{0.75}Fe_3(BO_3)_4$. Figure S8 Temperature dependencies of 1191 cm^{-1} Raman line position of $Sm_{0.25}La_{0.75}Fe_3(BO_3)_4$. Table S1. Calculated eigenvectors of the external vibrations (131, 178, 220, 302, 333, 445 cm^{-1}) (PDF)

■ AUTHOR INFORMATION

Corresponding Author

*E-mail: ekoles@iph.krasn.ru.

Notes

The authors declare no competing financial interest.

■ ACKNOWLEDGMENTS

This work was supported by the Russian Foundation for Basic Research, Project No. 14-02-00307.

■ REFERENCES

(1) Fausti, D.; Nugroho, A. A.; Van Loosdrecht, P. H. M.; Klimin, S. A.; Popova, M. N.; Bezmaternykh, L. N. *Phys. Rev. B: Condens. Matter Mater. Phys.* **2006**, *74*, 024403.

(2) Eremin, E. V.; Volkov, N. V.; Temerov, V. L.; Gudim, I. A.; Bovina, A. F. *Phys. Solid State* **2015**, *57* (3), 569−575.

(3) Chukalina, E. P.; Popova, M. N.; Bezmaternykh, L. N.; Gudim, I. A. *Phys. Lett. A* **2010**, *374*, 1790−1792.

(4) Chen, X.-B.; Thi Minh Hien, N.; Han; Kiok; Nam; Ji-Yeon; Thi Huyen, N.; Shin; Seong-II; Wang; Xueyun; Cheong, S. W.; Lee, D.; Noh, T. W.; Sung, N. H.; Cho, B. K.; Yang, I.-S. *Sci. Rep.* **2015**, *5*, 13366.

(5) Adem, U.; Wang, L.; Fausti, D.; Schottenhamel, W.; Van Loosdrecht, P. H. M.; Vasiliev, A.; Bezmaternykh, L. N.; Büchner, B.; Hess, C.; Klingeler, R. *Phys. Rev. B: Condens. Matter Mater. Phys.* **2010**, *82*, 064406.

(6) Krylov, A. S.; Sofronova, S. N.; Gudim, I. A.; Vtyurin, A. N. *Solid State Commun.* **2013**, *174*, 26−29.

(7) Gerasimova, Yu.V.; Sofronova, S. N.; Gudim, I. A.; Oreshonkov, A. S.; Vtyurin, A. N.; Ivanenko, A. A. *Phys. Solid State* **2016**, *58* (1), 155−159.

(8) Sofronova, S. N.; Gerasimova, Yu.V.; Vtyurin, A. N.; Gudim, I. A.; Shestakov, N. P.; Ivanenko, A. A. *Vib. Spectrosc.* **2014**, *72*, 20−25.

(9) Boldyrev, K. N.; Popova, M. N.; Bettinelli, M.; Temerov, V. L.; Gudim, I. A.; Bezmaternykh, L. N.; Loiseau, P.; Aka, G.; Leonyuk, N. I. *Opt. Mater.* **2012**, *34* (11), 1885−1889.

(10) Bezmaternykh, L. N.; Kharlamova, S. A.; Temerov, V. L. *Crystallogr. Rep.* **2004**, *49*, 855−857.

(11) Bezmaternykh, L. N.; Temerov, V. L.; Gudim, I. A.; Stolbovaya, N. A. *Crystallogr. Rep.* **2005**, *50* (1), 97−99.

(12) Krylov, A. S.; Kolesnikova, E. M.; Isaenko, L. I.; Krylova, S. N.; Vtyurin, A. N. *Cryst. Growth Des.* **2014**, *14*, 923−927.

(13) Krylov, A. S.; Sofronova, S. N.; Kolesnikova, E. M.; Ivanov, Yu.N.; Sukhovsky, A. A.; Goryainov, S. V.; Ivanenko, A. A.; Shestakov, N. P.; Kocharova, A. G.; Vtyurin, A. N. *J. Solid State Chem.* **2014**, *218*, 32−37.

(14) Malinovsky, V. K.; Pugachev, A. M.; Surovtsev, N. V. *Phys. Solid State* **2008**, *50* (6), 1137−1143.

(15) Smirnov, M. B.; Kazimirov, V. Yu. *LADY: Software for Lattice Dynamics Simulations*; Joint Institute for Nuclear Research Communications: Dubna, 2001.

(16) Pu, X. D.; Chen, J.; Shen, W. Z.; Ogawa, H.; Guo, Q. X. *J. Appl. Phys.* **2005**, *98*, 033527.

(17) Ritter, C.; Pankrats, A.; Gudim, I.; Vorotynov, A. *J. Phys.: Condens. Matter* **2012**, *24*, 386002.

DOI: 10.1021/acs.cgd.6b01079
Cryst. Growth Des. 2016, 16, 6915−6921